

# Chirality-induced Phonon Dispersion in a Noncentrosymmetric Micropolar Crystal

J. Kishine<sup>1,2</sup>, A. S. Ovchinnikov<sup>3,4</sup>, and A. A. Tereshchenko<sup>3</sup>

<sup>1</sup> *Division of Natural and Environmental Sciences,  
The Open University of Japan, Chiba, 261-8586, Japan*

<sup>2</sup> *Institute for Molecular Science, Okazaki, Aichi 444-8585, Japan*

<sup>3</sup> *Institute of Natural Sciences and Mathematics,*

*Ural Federal University, Ekaterinburg, 620083, Russia and*

<sup>4</sup> *Institute of Metal Physics, Ural Division, Russian Academy of Sciences, Ekaterinburg, 620219, Russia*

(Dated: November 6, 2020)

Features of the phonon spectrum of a chiral crystal are examined within the micropolar elasticity theory. This formalism accounts for not only translational micromotions of a medium but also rotational ones. It is found that there appears the phonon band splitting depending on the left/right-circular polarization in a purely phonon sector without invoking any outside subsystem. The phonon spectrum reveals parity breaking while preserving time-reversal symmetry, i.e. it possesses true chirality. We find that hybridization of the micro-rotational and translational modes gives rise to the acoustic phonon branch with a “roton” minimum reminiscent of the elementary excitations in the superfluid helium-4. We argue that a mechanism of this phenomena is in line with Nozières’ reinterpretation [J. Low Temp. Phys. **137**, 45 (2004)] of the rotons as a manifestation of an incipient crystallization instability. We discuss a close analogy between the translational and rotational micromotions in the micropolar elastic medium and the Bogoliubov quasiparticles and gapful density fluctuations in <sup>4</sup>He.

*Introduction.*— In hierarchy of electric, magnetic and mechanical degrees of freedom and attendant interrelationships namely mechanical and elastic properties of solids are most sensitive to structure. This is why the mechanical response in solids has recently been the target of a new branch of electronics, referred to as straintronics[1]. Connection of structural chirality with static and dynamical properties offers a key to understand functionality of chiral systems [2]. A quintessential example of the chirality-controlled phenomena is the optical activity[3], where propagation of circularly polarized light through a chiral material depends on its handedness. As for elastic degrees of freedom, a mechanical counterpart of optical activity, so-called acoustical activity, has been attracting revived attention[4]. This phenomena was first predicted by Portigal and Burstein[5] and direct observation thereof was subsequently provided for the  $\alpha$ -quartz crystal belonging to an enantiomorphic space group[6].

The acoustical activity is also related with first-order spatial dispersion contributions to the elastic constants [5]. This situation is somewhat similar to a role of Dzyaloshinskii-Moriya interaction which leads to a linear Lifshitz invariant in free energy of a chiral helimagnet [7, 8]. However, chirality effects are beyond the conventional elasticity theory [9], which considers only a local translation of points and the force stress (force per unit area) but completely ignores a local rotation of these points and the concomitant couple stress (a torque per unit area). As a consequence, there appears the elastic four-rank tensor,  $C_{ijkl}$ , which connects the parity-even and odd 2nd rank tensors, and gives rise to the chiral term in the energy functional ( $C_{klmn}\epsilon_{kl}\gamma_{mn}$  as explained below).

These missing effects, which may be viewed as a per-

ticular manifestation of nonlocality, are addressed in the micropolar elasticity theory[10, 11]. So far, only few attempts have been made to calculate dispersion curves of the micropolar elastic waves in crystals. We note in this regard the pioneering research undertaken by Pouget et al. for the centrosymmetric compound  $\text{KNO}_3$ [12], where spectrum of the micropolar waves reciprocal in the momentum space was obtained.

Then, the natural question arises as to whether a phonon spectrum in a chiral crystal exhibits non-reciprocity effects in propagation of micropolar elastic waves. This is the question addressed in this Letter. A salient feature of the nonreciprocity is a polarization-dependent splitting of phonon bands similar to the one for electronic bands due to spin-orbit coupling[13]. In contrast to the phonon magneto-chiral effect [14, 15], for which the splitting is achieved through coupling with nonreciprocal magnons, our aim is to find the result for a purely phononic sector without the involvement of any subsystem outside.

Another issue discussed in this Letter is how the structural chirality relates to the phonon angular momentum and spin. In this regard, we mention the recent studies of chiral phonons in monolayers of hexagonal [16] and kagome lattices [17]. In these systems, the phonon eigenmodes at high-symmetry points of the Brillouin zone (BZ) inherit the threefold rotational symmetry of the lattice which allows to label these phonon eigenmodes with pseudoangular momentum. It includes both orbital and spin parts, the latter coincides with the phonon chirality characterized by the circular polarization of phonons. In contrast to this scenario in which chirality is assigned only to special BZ points, we examine an effect of the structural chirality on phonon dispersion over the whole

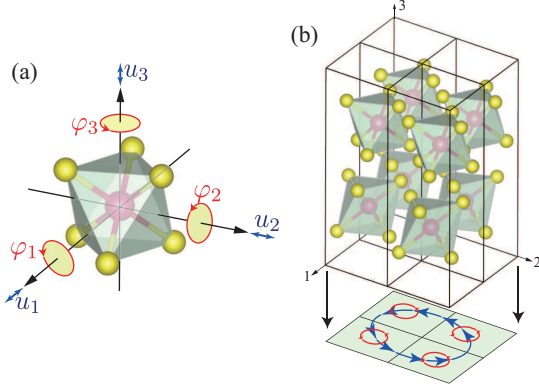


FIG. 1: (a) Schematic view of the rotational and translational degrees of freedom of the atomic microelement. As an example of the microelement, we show the  $\text{CrS}_6$  block inside the elementary cell of  $\text{CrNb}_3\text{S}_6$ . (b) Typical distribution of microrotation fields. We also depict conceptual representation of the micro-rotation (red small circle with arrows) and translation (blue large circle with arrows) associated with a circularly polarized mode, which are projected on the 1 – 2 plane.

Brillouin zone. The chiral helimagnet  $\text{CrNb}_3\text{S}_6$  serves to illustrate our results, one of which is striking similarity of microrotations embedded in the micropolar elasticity theory with roton excitations in helium-4.

*Chiral phonon dispersions for the point group 622.* – A general scheme of treatment of elementary excitations in the context of the micropolar elasticity theory may be found in Supplemental Material[18]. In this theory, the field of translational displacements,  $\mathbf{u}(\mathbf{r})$ , is supplemented by the field of microrotations,  $\boldsymbol{\varphi}(\mathbf{r})$ , and the both are attributed to a microelement located at the position  $\mathbf{r}$  (see Fig. 1). Two linear micropolar strain tensors  $\varepsilon_{kl} = \partial_l u_k - \varepsilon_{klm} \varphi_m$  and  $\gamma_{kl} = \partial_l \varphi_k$  form measures of microdeformations. Here and throughout,  $\varepsilon_{klm}$  is the Levi-Civita symbol and Einstein summation convention is used. The strain energy density is given by the quadratic form,  $U = \frac{1}{2} A_{klmn} \varepsilon_{kl} \varepsilon_{mn} + \frac{1}{2} B_{klmn} \gamma_{kl} \gamma_{mn} + C_{klmn} \varepsilon_{kl} \gamma_{mn}$ , where the third term (chiral term) changes its sign under the inversion operation while the first and the second do not. This chiral coupling leads to the left/right-circular-polarization-dependent non-reciprocal phonon dispersion.

To demonstrate how the chiral coupling gives rise to new peculiarities of phonon dispersion, we consider, as an example, the layered compound  $\text{CrNb}_3\text{S}_6$  which has the non-centrosymmetric hexagonal space group  $P6_322$ . In this material, the Cr atoms are intercalated between the sandwich layers S-Nb-S of the disulfide  $\text{NbS}_2$  and surrounded by the six S atoms in an octahedral geometry. The  $\text{CrS}_6$  octahedra are not linked to each other. The

distance  $d(\text{Cr-S}) = 2.393 \text{ \AA}$ [21] is less than  $\sim 0.1 \text{ \AA}$  the distance  $d(\text{Nb-S}) = 2.47 \div 2.50 \text{ \AA}$  [22]. Assuming that modes due to relative displacements of the Cr and S ions are not excited, the  $\text{CrS}_6$  may be modeled as a rigid structural unit. Below, we consider plane-waves propagating along the the crystalline [001] axis, i.e. the chiral axis.

Dispersion of the micropolar waves is obtained in the following way. To describe transverse modes, it is appropriate to introduce the circular basis,  $u_{\pm} = u_1 \pm iu_2$ , and  $\varphi_{\pm} = \varphi_1 \pm i\varphi_2$ , where  $+/-$  corresponds to the left/right circularly polarized microdeformation fields. Then, the EOMs for the decoupled transverse modes may be written as,

$$\rho \ddot{u}_{\pm} = A_{55} \partial_3^2 u_{\pm} + C_{74} \partial_3^2 \varphi_{\pm} \mp i (A_{47} - A_{55}) \partial_3 \varphi_{\pm}, \quad (1)$$

$$\begin{aligned} \rho j_{\pm} \ddot{\varphi}_{\pm} &= C_{74} \partial_3^2 u_{\pm} \mp i (A_{47} - A_{55}) \partial_3 u_{\pm} + B_{44} \partial_3^2 \varphi_{\pm} \\ &\mp 2i (C_{44} - C_{74}) \partial_3 \varphi_{\pm} - (A_{44} - 2A_{47} + A_{55}) \varphi_{\pm}, \end{aligned} \quad (2)$$

where  $\rho = 5.029 \text{ g/cm}^3$ [23] and  $j_{\pm} = j_{11} = 0.5 \times 10^{-19} \text{ m}^2$ [24] are the mass density and the microinertia tensor component, respectively. Here, the four-rank tensor elements are represented in the Sirotin (generalized Voigt) scheme[18]. The most important point is the appearance of the linear gradient terms,  $\partial_3 u_{\pm}$  and  $\partial_3 \varphi_{\pm}$ , which cause polarization-dependent velocities. Hybridization of these circularly polarized  $u_{\pm}$ - and  $\varphi_{\pm}$ -modes gives rise to acoustic and optical branches of the spectrum of propagating transverse waves in the micropolar medium. It is to be noted that each of the modes,  $u_{\pm}$  (or  $\varphi_{\pm}$ ), is non-reciprocal in real space, but they form a pair invariant under time-reversal symmetry. This may be inferred from Eqs. (1) and (2) which break parity  $\mathcal{P}$  but preserve time-reversal symmetry  $\mathcal{T}$ . This situation means that phonons in the micropolar chiral crystal exhibit *true chirality* in contrast to the phonon[14, 15] or electrical[25] magneto-chiral effects, where both  $\mathcal{P}$  and  $\mathcal{T}$  are simultaneously broken. On that understanding, we call these excitations truly chiral phonons. This polarization dependent splitting of the transverse phonon branches is analogous to the Rashba splitting of electronic bands, in which  $\mathcal{P}$  is also broken but not  $\mathcal{T}$ . Nonreciprocity of the truly chiral phonons originates from the  $(C_{44} - C_{74})$ -coupling term in the EOMs (1,2) and vanishes for  $C_{44} = C_{74}$ .

The equations that govern propagation of the longitudinal branches are written as

$$\rho \ddot{u}_3 = A_{33} \partial_3^2 u_3 + C_{33} \partial_3^2 \varphi_3, \quad (3)$$

$$\rho j_3 \ddot{\varphi}_3 = C_{33} \partial_3^2 u_3 + B_{33} \partial_3^2 \varphi_3 - 2(A_{66} - A_{69}) \varphi_3, \quad (4)$$

where  $j_3 = j_{33}$  will be taken as  $1.0 \times 10^{-19} \text{ m}^2$ . Note the absence of linear gradient terms that entails simple hybridization of the  $u_3$  and  $\varphi_3$  modes.

Phonon dispersion relations may be obtained inserting plane waves propagating along the chiral ( $x_3$ ) axis,

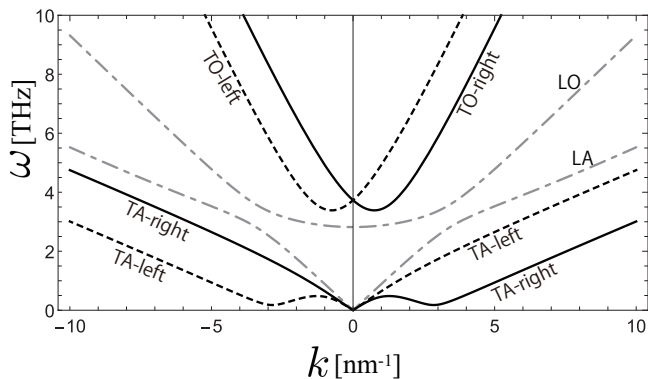


FIG. 2: Phonon dispersion curves for the chiral micropolar crystal: the longitudinal acoustic (LA) and optical (LO) branches (dashed-and-dotted line), the transverse left-handed acoustic (TA-left) and optical (TO-left) branches (dashed line), the transverse right-handed acoustic (TA-right) and optical (TO-right) branches (solid line). Numerical values of the tensor components are chosen as  $A_{33} = 0.4 \cdot 10^{10}$  N/m<sup>2</sup>,  $A_{66} = 4.9 \cdot 10^{10}$  N/m<sup>2</sup>,  $A_{69} = 4.7 \cdot 10^{10}$  N/m<sup>2</sup>,  $B_{33} = 1.5 \cdot 10^{-10}$  N,  $C_{33} = 0.3$  N/m for the longitudinal modes and  $A_{44} = 0.21 \cdot 10^{10}$  N/m<sup>2</sup>,  $A_{55} = 0.215 \cdot 10^{10}$  N/m<sup>2</sup>,  $A_{47} = 0.195 \cdot 10^{10}$  N/m<sup>2</sup>,  $B_{44} = 1.0 \cdot 10^{-10}$  N,  $C_{44} = 0.44$  N/m,  $C_{74} = 0.36$  N/m for the transverse modes, respectively.

$u_\alpha(x_3, t) = u_\alpha e^{i(kx_3 - \omega t)}$  and  $\varphi_\alpha(x_3, t) = \varphi_\alpha e^{i(kx_3 - \omega t)}$ , into Eqs. (1-4). Hereinafter, the index  $\alpha$  labels either the transverse-left/right (“+ / -”) circular or longitudinal (“3”) polarization of the phonon branches. The results are summarized in Fig. 2. There are six branches in total, namely, we have the longitudinal acoustic (LA)/optical (LO), the transverse left-handed acoustic (TA-left)/optical (TO-left), and the transverse right-handed acoustic (TA-right)/optical (TO-right) modes. The associated dispersion relations take the form

$$\left[ \omega_\alpha^{(O/A)} \right]^2 = \frac{1}{2\rho j_\alpha} \left[ b_\alpha + j_\alpha a_\alpha \pm \sqrt{(b_\alpha - j_\alpha a_\alpha)^2 + 4j_\alpha \Delta_\alpha^2} \right]. \quad (5)$$

The upper and lower  $\pm$  signs in the r.h.s. of Eq.(5) correspond to the optical (O) and acoustic (A) branches, respectively. The  $k$ -dependent parameters ( $a_\alpha$ ,  $b_\alpha$ , and  $\Delta_\alpha$ ) are given by  $a_\pm = A_{55}k^2$ ,  $b_\pm = B_{44}k^2 \mp 2(C_{44} - C_{74})k + (A_{44} + A_{55} - 2A_{47})$ ,  $\Delta_\pm = C_{74}k^2 \mp (A_{47} - A_{55})k$ , and  $a_3 = A_{33}k^2$ ,  $b_3 = B_{33}k^2 + 2(A_{66} - A_{69})$ ,  $\Delta_3 = C_{33}k^2$ . In the long wavelength limit,  $k \rightarrow 0$ , the frequencies of the acoustic branches are proportional to the wavenumber, while the frequencies of the optical branches tend to finite values,  $\omega_\pm^{(O)}(0) = \sqrt{(A_{44} + A_{55} - 2A_{47})/\rho j_\pm}$  and  $\omega_3^{(O)}(0) = \sqrt{(A_{66} - A_{69})/\rho j_3}$ .

*Similarity to roton spectrum.*— Figure 3 contains only the TA-right handed phonon mode specially selected from all branches shown in Fig. 2. We observe that hybridization of the rotational and translational modes

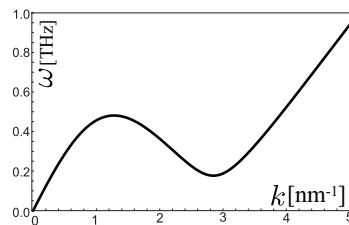


FIG. 3: The transverse right-handed acoustic (TA-right) branch that exhibits the roton-like minimum.

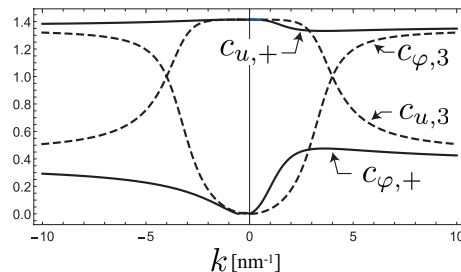


FIG. 4: The wavenumber dependence of the weights of translational and rotational modes in the hybridized TA-right (solid line) and LA (solid line) branches.

gives rise to the lowest phonon (TA-right or TA-left) branch which exhibits a “roton minimum” around  $k_m \sim (C_{44} - C_{74})/B_{44}$ , reminiscent of the excitation spectrum in superfluid<sup>4</sup>He [26]. The minimum occurs around a scale inversely proportional to the unit cell length and reflects hybridization of the rotational and translational degrees of freedom of the microelement CrS<sub>6</sub>.

To elucidate reasons behind an appearance of the roton-like minimum, we trace how translational and rotational modes contribute to the hybridized excitations. We find weights of these modes specified by the dimensionless coefficients  $c_{u,\alpha} = u_\alpha/\sqrt{J_\alpha}$  and  $c_{\varphi,\alpha} = \varphi_\alpha$ , whose explicit expressions are reproduced in Supplemental Material[18]. Their  $k$ -dependence is illustrated by Fig. 4 for the TA-right and LA branches. It is evident that the  $u_+ - \varphi_+$  hybridization causes resonant enhancement of the rotational degrees of freedom ( $\varphi_+$ ) when approaching the roton minimum. In contrast, the ratio between the coefficients  $c_{u,3}$  and  $c_{\varphi,3}$  is reversed near the crossing of the corresponding dispersion curves, which are modified into the hybridized LA and LO phonon modes.

There is actually an interesting parallel between the TA chiral phonons and roton excitations in superfluid<sup>4</sup>He. Originally, the rotons had been interpreted as a signature of some local vorticity. According to Feynman’s view[26], a maximum in the static form factor  $S_q$ , which signals a short range crystalline order, gives a roton minimum in the excitation spectrum through the relation  $\omega_q = q^2/2mS_q$ . Later, Nozières[27, 28] proposed an alternate scenario, where the rotons should be viewed

as an incipient soft mode associated with a crystallization instability. According to this view, the Bogoliubov quasiparticles hybridize with soft density fluctuations to cause a resultant roton minimum. The picture can be formulated by assuming two coupled excitations where the first correspond to the Bogoliubov quasiparticles with the spectrum  $\varepsilon_{\mathbf{q}}^B = [\xi_{\mathbf{q}}^2 + 2\xi_{\mathbf{q}}N_0U]^{1/2}$  and the second do to the density fluctuation mode, which is characterized by the single mode frequency  $\Omega_{\mathbf{q}}$ [27, 28]. Here,  $\xi_{\mathbf{q}}$  is the boson kinetic energy,  $N_0$  is a condensate fraction, and  $U$  is a direct repulsion between bosons. The spectrum of the hybridized quasiparticles has the form similar to Eq. (5),

$$E_{\mathbf{q}}^2 = \frac{1}{2} \left( \Omega_{\mathbf{q}}^2 + (\varepsilon_{\mathbf{q}}^B)^2 \right) \pm \frac{1}{2} \left[ \left( \Omega_{\mathbf{q}}^2 - (\varepsilon_{\mathbf{q}}^B)^2 \right)^2 + 16\alpha_{\mathbf{q}}^2 \xi_{\mathbf{q}} \Omega_{\mathbf{q}} \right]^{1/2}, \quad (6)$$

where  $\alpha_{\mathbf{q}}$  is a strength of coupling between the bosons and density fluctuations. Direct comparison between Eqs.(5) and (6) eloquently illustrates the one-to-one correspondence between the translational displacement,  $\mathbf{u}(\mathbf{r})$ , and the microrotation,  $\boldsymbol{\varphi}(\mathbf{r})$ , on one hand and the Bogoliubov quasiparticles and density fluctuations on the other [ $a_{\pm}(k)$  and  $b_{\pm}(k)$  respectively correspond to  $\varepsilon_{\mathbf{q}}^B$  and  $\Omega_{\mathbf{q}}$ ].

However, the roton minimum of the superfluid helium arises in the spectrum of the *longitudinal* sound wave of the normal component, while in the micropolar crystal this effect is observed in propagation of the *transversal* elastic waves, but not for the longitudinal ones. This difference may materialize arguments propounded by Landau and Feynman that the rotons are related to local vorticity [26]. The micro-rotation does warrant the name roton as spinning motion of the microelement.

There is further similarity between the rotons in  $^4\text{He}$  and the chiral phonons. The boson condensate lowers the roton minimum but the latter will remain finite due to the effect of condensate depletion[27, 28]. For the chiral phonons, a finite value of the roton minimum may be inferred from the requirement that the crystal must be stable against propagating elastic waves. In Supplemental Material[18], we give proof that the stability condition implies that the roton minimum will remain finite (never touch zero). An area of stability within the  $C_{44}$ - $C_{74}$  plane (these constants responsible for parity breaking) is plotted in Fig. 5, together with a region where the roton minimum emerges.

The roton minimum occurs around  $k \sim 3 \text{ nm}^{-1}$  roughly corresponds to 20 nm in real space, so the continuum theory developed here may be still be valid. The inelastic neutron or Brillouin light scattering measurements may potentially probe this finite  $k$  excitation. More quantitative arguments may require to build a bridge between the present continuum theory and atomic lattice

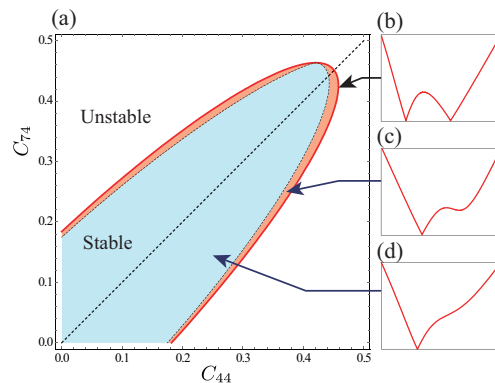


FIG. 5: (a) Phase diagram in the  $C_{44}$ - $C_{74}$  plane. The coloured area corresponds to stability of the crystal structure. The roton minimum appears in the vicinity of the soft mode instability (red). The concomitant profiles of the spectrum are shown on the right (b-d). Numerical parameters are the same as in Fig. 2.

model, which is left for future studies.

*Phonon angular momentum.*— Once the spectrum of the micropolar waves is known, one is capable to determine naturally orbital and spin parts of the angular momentum associated with elastic deformations. By specifying the basis of the left-handed ( $L$ ) and right-handed ( $R$ ) circularly polarized transverse modes as  $|R_u\rangle = |L_u\rangle^* = \frac{1}{\sqrt{2}}(1, i, 0, 0, 0, 0)^T$ , and  $|R_\varphi\rangle = |L_\varphi\rangle^* = \frac{1}{\sqrt{2}}(0, 0, 0, 1, i, 0)^T$  the solution  $|\mathbf{v}\rangle^T = (c_{u,1}, c_{u,2}, c_{u,3}, c_{\varphi,1}, c_{\varphi,2}, c_{\varphi,3})$  of Eqs. (1-4) may be decomposed as  $|\mathbf{v}\rangle = \sum_{\alpha=u,\varphi} \langle R_\alpha | \mathbf{v} \rangle |R_\alpha\rangle + \langle L_\alpha | \mathbf{v} \rangle |L_\alpha\rangle$ . Then, the generator of rotations of the phonon polarization plane around the  $z$ -axis, or phonon spin [16], is  $\hat{S}^z = \hbar \sum_{\alpha=u,\varphi} (|R_\alpha\rangle \langle R_\alpha| - |L_\alpha\rangle \langle L_\alpha|)$ , so that

$$\langle \mathbf{v} | \hat{S}^z | \mathbf{v} \rangle = \frac{\hbar}{2} \sum_{f=u,\varphi} (|c_{f,-}|^2 - |c_{f,+}|^2) \quad (7)$$

is fulfilled. Obviously, the phonon circular polarization is quantized, i.e. it can take only the  $\pm\hbar$  values for the “ $\mp$ ”-branches, respectively. Unlike chiral phonons in the theories[16, 17], the phonon spin is introduced for any  $k$ -point of the Brillouin zone. Neglecting the microrotations  $\boldsymbol{\varphi}$ , the definition coincides with the spin part of the phonon angular momentum given in Ref.[29],  $\mathbf{L}_s = \hbar \sum_{\mathbf{k}} \mathbf{e}_{\mathbf{k}} (a_{\mathbf{k}-}^\dagger a_{\mathbf{k}-} - a_{\mathbf{k}+}^\dagger a_{\mathbf{k}+})$ , where the angular momenta  $\hbar$  of the individual ( $\mathbf{k}\pm$ )-phonons add up either parallel or anti-parallel to their wave vectors,  $\mathbf{e}_{\mathbf{k}} = \mathbf{k}/|\mathbf{k}|$ . Classical interpretation of the resultant  $\mathbf{L}_s$  corresponds to small-radius circular shear displacements of points around their equilibrium positions [Fig. 1(b)].

With regard to the orbital part of the phonon angular momentum, its definition,  $L_{\pm} = \rho j_{\pm} \dot{\varphi}_{\pm}$ , follows directly from the appropriate conservation law of the micropolar

theory[10]. This implies propagation of plane waves of the angular momentum density.

*Roton and acoustic activity.*—Nonreciprocity of the chiral phonons results in consequential acoustic activity, most notably in the vicinity of the roton minimum. By definition, the effect occurs when incident transverse acoustic waves, which are lineally polarized, propagate in the crystal along the  $z$ -axis. It is characterized by the rotation angle,  $\phi = \frac{1}{2}\omega l(1/v_- - 1/v_+)$ , at a distance  $l$  from the incident surface. The phase velocities  $v_{\pm}$  of the circularly polarized transverse modes may be calculated from the dispersion relations (5) to give

$$\frac{\phi}{l} = \rho\omega^2 \frac{(A_{47} - A_{55})}{(A_{44}A_{55} - A_{47}^2)^2} \times [A_{55}C_{44} + A_{44}C_{74} - A_{47}(C_{44} + C_{74})]. \quad (8)$$

Comparison with EOMs (1,2) shows that apart from the intercross coupling  $A_{55} - A_{47}$  between the micro-translations and microrotations, the inherent gyrotropy  $C_{44} - C_{74}$  of the microrotations is an essential element of acoustic activity. Unlike the micropolar theory, the conventional approach [5, 6] relates the latter to non-local interaction between stress and strain; this is reflected in the first-order dispersion in expansion of the elastic coefficients  $c_{ij}(\mathbf{k}, \omega)$ . As a consequence, a difference in phase velocities of circularly polarized waves appears at any  $\mathbf{k}$  vector.

*Concluding remarks.*—We demonstrate polarization-dependent splitting of phonon bands in a chiral crystal, using the micropolar elasticity theory for  $\text{CrNb}_3\text{S}_6$ . Our main results may be summarized as follows. (I) The splitting is reached solely within the phonon sector of elementary excitations, and it is maintained by coupling between the transverse translational and rotational modes of the micropolar medium. (II) Transverse acoustic branches of the hybridized phonon spectrum exhibit a “roton” minimum reminiscent of elementary excitations in the superfluid helium-4. We argue that the translational and rotational degrees of freedom of the chiral phonon system correspond to the Bogoliubov quasiparticles and massive density fluctuations, respectively, in the superfluid helium-4. In addition, we discuss acoustic activity originated from nonreciprocity of the phonon spectrum. It is expected that the polarization-dependent phonon dispersions demonstrated may lead to chirality-induced cross correlations among lattice, electronic and magnetic degrees of freedom.

The authors give special thanks to Yusuke Kato for directing our attention to Ref.[27, 28]. We thank Laurence Barron for continuous encouragement. We also thank Nikolay Baranov, Yoshihiko Togawa and Hiroshi Yamamoto for stimulating discussions concerning experimental insights. The authors acknowledge JSPS Bilateral Joint Research Projects (JSPS-RFBR), the Russian Foundation for Basic Research (RFBR), Grant 20-52-

50005. This work was supported by JSPS KAKENHI Grant Number 17H02923. A.S.O. acknowledges funding by Act 211 Government of the Russian Federation, Contract No. 02.A03.21.0006, and the Ministry of Education and Science of Russia, Project No. FEUZ-2020-0054.

- 
- [1] A.A. Bukharaev, A.K. Zvezdin, A.P. Pyatakov, and Y.K. Fetisov, *Phys.-Usp.* **61**, 1175 (2018).
  - [2] L. D. Barron, *Chirality* **24**, 879 (2012).
  - [3] L. D. Barron, *Molecular Light Scattering and Optical Activity*, 2nd ed., (Cambridge University Press, Cambridge, U.K., 2004).
  - [4] Tobias Frenzel, Julian Köfler, Erik Jung, Muamer Kadic, and Martin Wegener, *Nat. Commun.* **10**, 3384 (2019); I. Fernandez-Corbaton, C. Rockstuhl, P. Ziemke, P. Gumbusch, A. Albiez, R. Schwaiger, T. Frenzel, M. Kadic, and M. Wegener, *Adv. Mater.* **31**, 1807742 (2019).
  - [5] D.L. Portigal and E. Burstein, *Phys. Rev.* **170**, 673 (1968).
  - [6] A.S. Pine, *J. Acoust. Soc. Amer.* **49**, 1026 (1971).
  - [7] J. Kishine and A. S. Ovchinnikov, *Solid State Phys.* **66**, 1 (2015).
  - [8] G.W. Paterson, A.A. Tereshchenko, S. Nakayama, Y. Kousaka, J. Kishine, S. McVitie, A.S. Ovchinnikov, I. Proskurin, and Y. Togawa, *Phys. Rev. B* **101**, 184424 (2020).
  - [9] L.D. Landau and E. M. Lifshitz, *Theory of Elasticity* (Butterworth-Heinemann, Oxford, 1986).
  - [10] A.C. Eringen, *Microcontinuum Field Theories: I. Foundations and Solids* (Springer-Verlag, New York, 1999).
  - [11] W. Nowacki, *Theory of asymmetric elasticity* (Pergamon Press, Oxford, 1986).
  - [12] J. Pouget, A. Aşar, G.A. Maugin, *Phys. Rev. B* **33**, 6304 (1986); **33**, 6320 (1986).
  - [13] E. I. Rashba and V. I. Sheka, *Fiz. Tverd. Tela* **1**, 162-176 (1959) (in Russian); G. Bihlmayer, O. Rader, and R. Winkler, *New J. Phys.* **17**, 050202 (2015).
  - [14] A.A. Tereshchenko, A.S. Ovchinnikov, I. Proskurin, E.V. Sinitsyn, and J. Kishine, *Phys. Rev. B* **97**, 184303 (2018).
  - [15] T. Nomura, X.-X. Zhang, S. Zherlitsyn, J. Wosnitza, Y. Tokura, N. Nagaosa, and S. Seki, *Phys. Rev. Lett.* **122**, 145901 (2019).
  - [16] L. Zhang and Q. Niu, *Phys. Rev. Lett.* **115**, 115502 (2015); H. Zhu, J. Yi, M.-Y. Li, J. Xiao, L. Zhang, C.-W. Yang, R. A. Kaindl, L.-J. Li, Y. Wang, and X. Zhang, *Science* **359**, 579–582 (2018).
  - [17] H. Chen, W. Wu, S. A. Yang, X. Li, and L. Zhang, *Phys. Rev. B* **100**, 094303 (2019).
  - [18] See Supplemental Material at <http://link.aps.org/supplemental/XXX/PhysRevLett.XXX>, which includes Ref. [19, 20].
  - [19] H. A. Jahn, *Acta Crystallogr.* **2**, 33 (1949).
  - [20] Y.I. Sirotin, M.P. Shaskolskaya, *Fundamentals of Crystal Physics* (Mir, Moscow, 1982).
  - [21] L.M. Volkova and D.V. Marinin, *J. Appl. Phys.* **116**, 133901 (2014).
  - [22] P.R. Sarode, *Phys. Status Solidi A* **98**, 391 (1986).
  - [23] N.J. Ghimire, M.A. McGuire, D.S. Parker, B. Sipos, S. Tang, J.-Q. Yan, B.C. Sales, and D. Mandrus, *Phys. Rev. B* **87**, 104403 (2013).

- [24] The order of the microinertia tensor is ensued from the definition  $j_{kl} = \langle \xi_k \xi_l \rangle$ , where  $\boldsymbol{\xi}$  is the microdeformation coordinate (f.e., see Ref.[10]).
- [25] R. Aoki, Y. Kousaka, and Y. Togawa, Phys. Rev. Lett. **122**, 057206 (2019).
- [26] L. Landau, Phys. Rev. **60**, 356 (1941); R.P. Feynman, Rev. Mod. Phys. **29**, 205 (1957).
- [27] P. Nozières, J. Low Temp. Phys. **137**, 45 (2004).
- [28] P. Nozières, J. Low Temp. Phys. **142**, 91 (2006).
- [29] D.A. Garanin and E.M. Chudnovsky, Phys. Rev. B **92**, 024421 (2015).

# Supplementary Material for: Chirality-induced Phonon Dispersion in a Noncentrosymmetric Micropolar Crystal

J. Kishine, A. S. Ovchinnikov, and A. A. Tereshchenko

In this Supplementary Material we present technical details related to the micropolar elasticity theory. In Sec. I, we summarize a general formulation. In Sec. II, a concrete form of equations of motion is derived for the 622 point group. In Sec. III, the stability condition and a finite gap of the roton minimum are discussed.

## GENERAL FORMULATION

In the linear micropolar continuum, the displacement field vector  $\mathbf{u}$  is supplemented by the microrotation field vector  $\boldsymbol{\varphi}$ , *which are independent of each other*[10,11]. Strain measures of the micropolar media are described by two tensors, i.e. the microdeformation tensor

$$\varepsilon_{kl} = \partial_l u_k - \epsilon_{klm} \varphi_m, \quad (1)$$

and the wryness (microrotation) tensor

$$\gamma_{kl} = \partial_l \varphi_k, \quad (2)$$

where  $\epsilon_{klm}$  is the totally antisymmetric tensor (Levi-Civita symbol) and the Einstein summation convention is used. The microdeformation tensor  $\varepsilon_{kl}$  is even under the inversion operation because  $\partial_l$  and  $u_k$  are polar while  $\varphi_m$  is axial. On the other hand, the wryness tensor  $\gamma_{kl}$  is odd.

Note that the microdeformation tensor  $\varepsilon_{kl}$  is different from conventional Cauchy's strain tensor,  $\frac{1}{2}(\partial_l u_k + \partial_k u_l)$ . To see the difference, it is useful to note that  $\partial_l u_k$  can be always decomposed into a symmetric and antisymmetric parts,

$$\partial_l u_k = \underbrace{\frac{1}{2}(\partial_l u_k + \partial_k u_l)}_{\text{Cauchy's strain } \varepsilon_{kl}^C} + \frac{1}{2}(\partial_l u_k - \partial_k u_l) = \varepsilon_{kl}^C + \epsilon_{klm} \omega_m, \quad (3)$$

where  $\varepsilon_{kl}^C$  denotes the Cauchy's strain tensor and  $\omega_m$  does the axial rotation vector. Rewriting this relation as

$$\varepsilon_{kl}^C = \partial_l u_k - \epsilon_{klm} \omega_m, \quad (4)$$

the difference between  $\varepsilon_{kl}$  and  $\varepsilon_{kl}^C$  becomes clear. In the conventional elasticity theory, the axial rotation vector,  $\boldsymbol{\omega}$ , originates from the translational displacement,  $\mathbf{u}$ , similar to  $\varepsilon_{kl}^C$ , and describes rotation around the origin, the Cr-ion position[see Fig. 1(b)]. On the other hand, in the Cosserat (micropolar) theory, the microrotation vector,  $\boldsymbol{\varphi}$ , is totally independent of  $\mathbf{u}$ .

The strain energy density is given by the quadratic form[10,11],  $U = \frac{1}{2}A_{klmn}\varepsilon_{kl}\varepsilon_{mn} + \frac{1}{2}B_{klmn}\gamma_{kl}\gamma_{mn} +$

$C_{klmn}\varepsilon_{kl}\gamma_{mn}$ . The four-rank tensors  $\mathbf{A}$  and  $\mathbf{B}$  are both polar tensors and exist irrespective of inversion symmetry. They possess the property  $A_{klmn} = A_{mnlk}$  and  $B_{klmn} = B_{mnlk}$ , which has an internal symmetry  $[(V)^2]^2$  in Jahn's symbol[19]. The pseudotensor  $\mathbf{C}$  has an internal symmetry  $V^4$  and exists only in crystals without inversion symmetry. It provides interaction between the parity-even  $\varepsilon_{kl}$  and parity-odd  $\gamma_{kl}$ . This 'translation-rotation' coupling is the essential feature of chirality as has been highlighted in the Introduction. A number of independent elements of the  $A_{klmn}$  ( $B_{klmn}$ ) and  $C_{klmn}$  conditioned by permutations of the indices amounts to 45 and 81, respectively. A further account of the point group symmetry of a given crystal reduces their number. In addition, the tensor components must maintain positive definiteness of the internal energy,  $U > 0$ , for all strains to guarantee stability of the ground state against elementary excitations (phonons). Using the lattice theory [12], whereby atomic interactions are modelled by springs, typical magnitudes of the tensor components amount at most to  $A_{klmn} \sim 10^{10} \text{ N} \cdot \text{m}^{-2}$ ,  $B_{klmn} \sim 10^{-10} \text{ N}$  and  $C_{klmn} \sim 10^0 \text{ N} \cdot \text{m}^{-1}$ .

Variation of  $U$  with respect to  $\varepsilon_{kl}$  leads to the linear constitutive equation for the stress tensor,  $t_{kl} = \delta U / \delta \varepsilon_{lk} = A_{klmn} \varepsilon_{mn} + C_{klmn} \gamma_{mn}$ . Similarly, one obtains the couple stress tensor  $m_{kl} = \delta U / \delta \gamma_{kl} = C_{mnlk} \varepsilon_{mn} + B_{lkmn} \gamma_{mn}$ .

Now consider an elastic body occupying a region of volume  $\mathcal{V}$  bounded by the body surface  $\partial\mathcal{V}$ . The torque exerted on an element of the surface area reads a

$$d\mathbf{S} = \hat{\mathbf{n}} dS \quad (5)$$

with the exterior normal  $\hat{\mathbf{n}}$  to  $\partial\mathcal{V}$ .

The total torque acting on this surface microelement includes the orbital torque,  $\mathbf{x} \times \mathbf{T}$ , and the spin torque,  $\mathbf{M}$ , where  $\mathbf{T}$  denotes a force acting on  $dS$ . Then, we have

$$(\mathbf{x} \times \mathbf{T} + \mathbf{M})_\alpha dS = \epsilon_{\alpha\beta\gamma} x_\beta T_\gamma dS + M_\alpha dS. \quad (6)$$

The vectors  $\mathbf{T}$  and  $\mathbf{M}$  may be rewritten via the force stress and coupled stress tensors as

$$T_\gamma = t_{\delta\gamma} \hat{n}_\delta, \quad M_\alpha = m_{\delta\alpha} \hat{n}_\delta. \quad (7)$$

We shall restrict our discussion to a case when there is neither external volume force nor volume torque. Then, the rate of change of the angular momentum results from the orbital and spin torques acting on the microelement



Table 22 of Ref. [20] gives  $\mathbf{C}$  in the form summarized in Table II. It is readily seen that a number of independent elements equals to 10:  $C_{12}, C_{13}, C_{31}, C_{33}, C_{44}, C_{47}, C_{55}, C_{74}, C_{66}, C_{69}$ .

	11	22	33	23	31	12	32	13	21
11	$C_{11}$	$C_{12}$	$C_{13}$	0	0	0	0	0	0
22	$C_{12}$	$C_{11}$	$C_{13}$	0	0	0	0	0	0
33	$C_{31}$	$C_{31}$	$C_{33}$	0	0	0	0	0	0
23	0	0	0	$C_{44}$	0	0	$C_{47}$	0	0
31	0	0	0	0	$C_{55}$	0	0	$C_{74}$	0
12	0	0	0	0	0	$C_{66}$	0	0	$C_{69}$
32	0	0	0	$C_{74}$	0	0	$C_{55}$	0	0
13	0	0	0	0	$C_{47}$	0	0	$C_{44}$	0
21	0	0	0	0	0	$C_{69}$	0	0	$C_{66}$

TABLE II: Nonzero tensor components of  $\mathbf{C}$  for the point group 622. There is the constraint  $C_{11} = C_{12} + C_{66} + C_{69}$ .

## PHONON DISPERSIONS

### Transverse branches

Making use data from Tables I and II an explicit form of the equations of motion comes from Eqs. (13,14). The microinertia tensor can be written in the diagonal form  $\hat{j} = \text{diag}(j_1, j_1, j_3)$  by taking into account the almost  $3\bar{m}$  ( $D_{3d}$ ) point group symmetry of the CrS<sub>6</sub> block. This leads to

$$\rho\ddot{u}_1 = A_{55}\partial_3^2 u_1 - (A_{55} - A_{47})\partial_3\varphi_2 + C_{74}\partial_3^2\varphi_1, \quad (22)$$

$$\rho\ddot{u}_2 = A_{55}\partial_3^2 u_2 - (A_{47} - A_{55})\partial_3\varphi_1 + C_{74}\partial_3^2\varphi_2, \quad (23)$$

$$\rho\ddot{u}_3 = A_{33}\partial_3^2 u_3 + C_{33}\partial_3^2\varphi_3, \quad (24)$$

$$\begin{aligned} \rho j_1 \ddot{\varphi}_1 &= C_{74}\partial_3^2 u_1 + 2(C_{44} - C_{74})\partial_3\varphi_2 + B_{44}\partial_3^2\varphi_1 \\ &+ (A_{47} - A_{55})\partial_3 u_2 - (A_{44} - 2A_{47} + A_{55})\varphi_1, \end{aligned} \quad (25)$$

$$\begin{aligned} \rho j_1 \ddot{\varphi}_2 &= C_{74}\partial_3^2 u_2 - 2(C_{44} - C_{74})\partial_3\varphi_1 + B_{44}\partial_3^2\varphi_2 \\ &- (A_{47} - A_{55})\partial_3 u_1 - (A_{44} - 2A_{47} + A_{55})\varphi_2, \end{aligned} \quad (26)$$

$$\rho j_3 \ddot{\varphi}_3 = C_{33}\partial_3^2 u_3 + B_{33}\partial_3^2\varphi_3 - 2(A_{66} - A_{69})\varphi_3. \quad (27)$$

To simplify a solution of the equations of motion, the linearly polarized fields are relaxed by

$$u_{\pm} = u_1 \pm iu_2, \quad (28)$$

$$\varphi_{\pm} = \varphi_1 \pm i\varphi_2 \quad (29)$$

that are circularly polarized and counterrotating in the (1, 2) plane. The sign  $+$ ( $-$ ) corresponds to the left (right) circular polarization.

In the chiral basis the EOMs for the transverse modes are

$$\rho\ddot{u}_{\pm} = A_{55}\partial_3^2 u_{\pm} + C_{74}\partial_3^2\varphi_{\pm} \mp i(A_{47} - A_{55})\partial_3\varphi_{\pm}, \quad (30)$$

$$\begin{aligned} \rho j_{\pm} \ddot{\varphi}_{\pm} &= C_{74}\partial_3^2 u_{\pm} \mp i(A_{47} - A_{55})\partial_3 u_{\pm} + B_{44}\partial_3^2\varphi_{\pm} \\ &\mp 2i(C_{44} - C_{74})\partial_3\varphi_{\pm} - (A_{44} - 2A_{47} + A_{55})\varphi_{\pm}, \end{aligned} \quad (31)$$

where  $j_+ = j_- = j_1$ .

To get a dispersion relation, we use the plane-wave solutions

$$u_{\alpha}(x_3, t) = U_{\alpha}e^{-i(\omega t - kx_3)}, \quad \varphi_{\alpha}(x_3, t) = \Phi_{\alpha}e^{-i(\omega t - kx_3)}, \quad (32)$$

where the index  $\alpha$  labels  $+$ ,  $-$  and  $3$ .

The EOMs for the transverse modes ( $\alpha = \pm$ ) are written in the matrix form as

$$\begin{pmatrix} \rho\omega_{\alpha}^2 - a_{\alpha} & -\Delta_{\alpha} \\ -\Delta_{\alpha} & \rho j_{\alpha}\omega_{\alpha}^2 - b_{\alpha} \end{pmatrix} \begin{pmatrix} U_{\alpha} \\ \Phi_{\alpha} \end{pmatrix} = 0. \quad (33)$$

Here, the  $k$ -dependent coefficients are introduced

$$a_{\pm} = A_{55}k^2, \quad (34)$$

$$\begin{aligned} b_{\pm} &= B_{44}k^2 \mp 2(C_{44} - C_{74})k \\ &+ (A_{44} + A_{55} - 2A_{47}), \end{aligned} \quad (35)$$

$$\Delta_{\pm} = C_{74}k^2 \pm (A_{55} - A_{47})k. \quad (36)$$

It is immediately recognized that the crystal has two branches for each polarization  $\alpha$ :

(I) the acoustic branch

$$\omega_{\alpha}^{(A)}(k)^2 = \frac{1}{2\rho j_{\alpha}} \left[ b_{\alpha} + j_{\alpha}a_{\alpha} - \sqrt{(b_{\alpha} - j_{\alpha}a_{\alpha})^2 + 4j_{\alpha}\Delta_{\alpha}^2} \right]; \quad (37)$$

(II) the optical branch

$$\omega_{\alpha}^{(O)}(k)^2 = \frac{1}{2\rho j_{\alpha}} \left[ b_{\alpha} + j_{\alpha}a_{\alpha} + \sqrt{(b_{\alpha} - j_{\alpha}a_{\alpha})^2 + 4j_{\alpha}\Delta_{\alpha}^2} \right]. \quad (38)$$

The acoustic branch starts off at zero frequency, while the optical branch starts off at some finite value

$$\omega_{\pm}^{(A)}(0)^2 = 0, \quad \omega_{\pm}^{(O)}(0)^2 = \frac{1}{\rho j_{\pm}} (A_{44} + A_{55} - 2A_{47}). \quad (39)$$

### Longitudinal branches

It is to be noted that the transverse and longitudinal modes are totally decouple. The EOMs for the longitudinal modes read

$$\rho\ddot{u}_3 = A_{33}\partial_3^2 u_3 + C_{33}\partial_3^2\varphi_3, \quad (40)$$

$$\rho j_3 \ddot{\varphi}_3 = C_{33}\partial_3^2 u_3 + B_{33}\partial_3^2\varphi_3 - 2(A_{66} - A_{69})\varphi_3. \quad (41)$$

By repeating the procedure presented above one obtains the acoustic and optical branches given by Eqs. (37,38), where  $\alpha = 3$  and

$$a_3 = A_{33}k^2, \quad (42)$$

$$b_3 = B_{33}k^2 + 2(A_{66} - A_{69}), \quad (43)$$

$$\Delta_3 = C_{33}k^2. \quad (44)$$

At  $k = 0$  we have

$$\omega_3^{(A)}(0)^2 = 0, \quad \omega_3^{(O)}(0)^2 = \frac{2}{\rho j_3} (A_{66} - A_{69}). \quad (45)$$

### Weights of the transverse $u$ and $\varphi$ modes

The EOMs (33) can be recast in the equivalent form

$$\begin{pmatrix} j_\alpha^{1/2} (\rho\omega_\alpha^2 - a_\alpha) & -\Delta_\alpha \\ -j_\alpha^{1/2} \Delta_\alpha & (\rho j_\alpha \omega_\alpha^2 - b_\alpha) \end{pmatrix} \times \begin{pmatrix} j_\alpha^{-1/2} U_\alpha \\ \Phi_\alpha \end{pmatrix} = 0, \quad (46)$$

where both  $j_\alpha^{-1/2} U_\alpha$  and  $\Phi_\alpha$  are dimensionless, since  $j_\alpha^{1/2}$  has a length scale of order of the microelement size.

Inserting in this equation the relation

$$\rho\omega_\alpha^2 - a_\alpha = \frac{1}{2j_\alpha} \left[ b_\alpha - j_\alpha a_\alpha \mp \sqrt{(b_\alpha - j_\alpha a_\alpha)^2 + 4j_\alpha \Delta_\alpha^2} \right], \quad (47)$$

we obtain

$$\begin{aligned} j_\alpha^{-1/2} |U_\alpha| &= \left[ \frac{1}{2} + \frac{j_\alpha (a_\alpha - \rho\omega_\alpha^2)^2}{2\Delta_\alpha^2} \right]^{-1/2} \\ &= \left[ \frac{1}{2} + \frac{\left( b_\alpha - j_\alpha a_\alpha \mp \sqrt{(b_\alpha - j_\alpha a_\alpha)^2 + 4j_\alpha \Delta_\alpha^2} \right)^2}{8j_\alpha \Delta_\alpha^2} \right]^{-1/2}, \end{aligned} \quad (48)$$

where the upper/lower sign corresponds to the acoustic/optical branch.

Analogously, we get

$$\begin{aligned} |\Phi_\alpha| &= \left[ \frac{1}{2} + \frac{\Delta_\alpha^2}{2j_\alpha (a_\alpha - \rho\omega_\alpha^2)^2} \right]^{-1/2} \\ &= \left[ \frac{1}{2} + \frac{2j_\alpha \Delta_\alpha^2}{\left( b_\alpha - j_\alpha a_\alpha \mp \sqrt{(b_\alpha - j_\alpha a_\alpha)^2 + 4j_\alpha \Delta_\alpha^2} \right)^2} \right]^{-1/2}, \end{aligned} \quad (49)$$

where the normalization condition

$$\left| \frac{j_\alpha^{-1/2} U_\alpha}{\sqrt{2}} \right|^2 + \left| \frac{\Phi_\alpha}{\sqrt{2}} \right|^2 = 1 \quad (50)$$

is accounted for.

In Fig. S1, we show the dispersion curves of the TA-right branch and corresponding weights. It is clearly seen that the roton minimum is correlated to the depletion of the  $u+$  mode and complementary evolution of the  $\varphi+$  mode.

### STABILITY CONDITION AND ROTON MINIMUM

Below we formulate the condition of ground state stability against phonon excitations. For this purpose, we write down the energy  $U$  by retaining only those tensor components which appear in the equations of motion for the case of the point group 622

$$\begin{aligned} U &= \frac{1}{2} (A_{66} + A_{69}) (\varepsilon_{11}^2 + \varepsilon_{22}^2) + \frac{1}{2} A_{66} (\varepsilon_{12}^2 + \varepsilon_{21}^2) \\ &\quad + A_{69} \varepsilon_{12} \varepsilon_{21} + \frac{1}{2} A_{33} \varepsilon_{33}^2 + C_{33} \varepsilon_{33} \gamma_{33} + \frac{1}{2} B_{33} \gamma_{33}^2 \\ &\quad + \frac{1}{2} A_{44} (\varepsilon_{23}^2 + \varepsilon_{13}^2) + A_{47} (\varepsilon_{32} \varepsilon_{23} + \varepsilon_{31} \varepsilon_{13}) \\ &\quad + C_{44} (\varepsilon_{23} \gamma_{23} + \varepsilon_{13} \gamma_{13}) \\ &\quad + \frac{1}{2} A_{55} (\varepsilon_{32}^2 + \varepsilon_{31}^2) + C_{74} (\varepsilon_{31} \gamma_{13} + \varepsilon_{32} \gamma_{23}) \\ &\quad + \frac{1}{2} B_{44} (\gamma_{23}^2 + \gamma_{13}^2), \end{aligned} \quad (51)$$

where we used

$$A_{11} = A_{66} + A_{69}, \quad C_{11} = C_{66} + C_{69}. \quad (52)$$

Introducing the vectors

$$\begin{aligned} \boldsymbol{\eta}_1 &= (\varepsilon_{11}, \varepsilon_{22})^T, \boldsymbol{\eta}_2 = (\varepsilon_{12}, \varepsilon_{21})^T, \boldsymbol{\eta}_3 = (\varepsilon_{33}, \gamma_{33})^T, \\ \boldsymbol{\eta}_4 &= (\varepsilon_{23}, \varepsilon_{32}, \gamma_{23})^T, \boldsymbol{\eta}_5 = (\varepsilon_{13}, \varepsilon_{31}, \gamma_{13})^T, \end{aligned} \quad (53)$$

the stability condition reads

$$U = \frac{1}{2} \sum_{i=1}^5 \boldsymbol{\eta}_i^T \hat{\mathbf{M}}_i \boldsymbol{\eta}_i > 0, \quad (54)$$

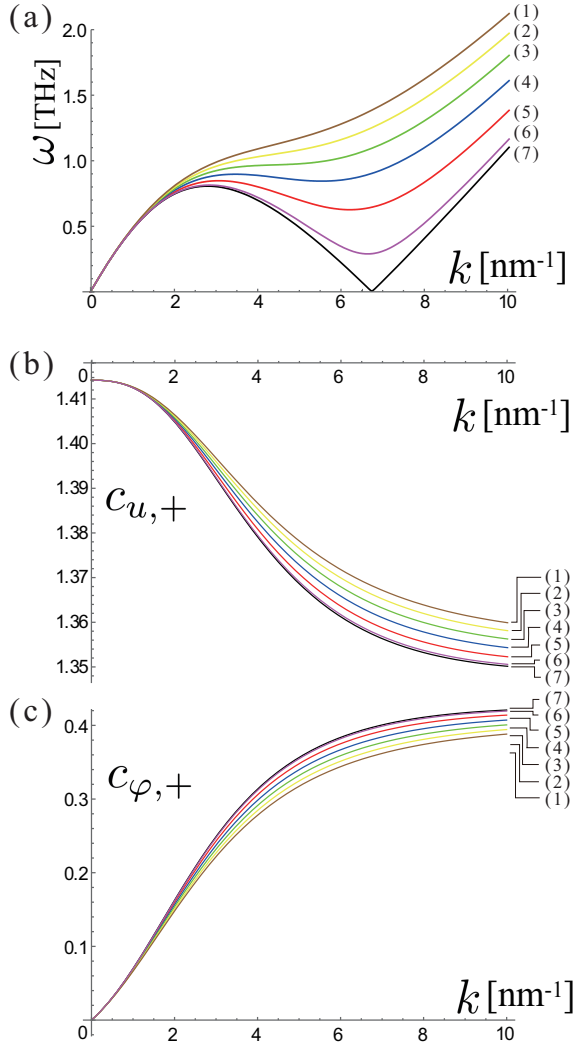


FIG. S1: Phonon dispersion curves for the chiral micropolar crystal: the longitudinal acoustic (LA) and optical (LO) branches (green dotted), the transverse left-handed acoustic (TA-left) and optical (TO-left) branches (blue solid), the transverse right-handed acoustic (TA-right) and optical (TO-right) branches (red solid). The wavenumber dependence of the weights of translational and rotational modes in the hybridized TA-right (red solid) and LA (green dotted) branches.  $A_{44} = 0.2 \cdot 10^{10}$  N/m<sup>2</sup>,  $A_{55} = 0.2 \cdot 10^{10}$  N/m<sup>2</sup>,  $A_{47} = 0.11 \cdot 10^{10}$  N/m<sup>2</sup>,  $B_{44} = 0.92115 \cdot 10^{-10}$  N, and  $C_{74} = 0.35$  N/m.  $C_{44} = (1) 0.35, (2) 0.36, (3) 0.37, (4) 0.38, (5) 0.39, (6) 0.398,$  and  $(7) 0.40$  in the unit of N/m.

where the matrices are

$$\hat{\mathbf{M}}_1 = \begin{pmatrix} A_{66} + A_{69} & 0 \\ 0 & A_{66} + A_{69} \end{pmatrix}, \quad (55)$$

$$\hat{\mathbf{M}}_2 = \begin{pmatrix} A_{66} & A_{69} \\ A_{69} & A_{66} \end{pmatrix}, \quad (56)$$

$$\hat{\mathbf{M}}_3 = \begin{pmatrix} A_{33} & C_{33} \\ C_{33} & B_{33} \end{pmatrix}, \quad (57)$$

$$\hat{\mathbf{M}}_4 = \hat{\mathbf{M}}_5 = \hat{\mathbf{M}} = \begin{pmatrix} A_{44} & A_{47} & C_{44} \\ A_{47} & A_{55} & C_{74} \\ C_{44} & C_{74} & B_{44} \end{pmatrix}. \quad (58)$$

This condition ensures that all eigenvalues of the  $\hat{\mathbf{M}}$ -matrices are positive. The terms that contain  $\hat{\mathbf{M}}_4 = \hat{\mathbf{M}}_5 = \hat{\mathbf{M}}$  are of particular importance.

Now, we relate the stability condition with the impossibility of zeroing of the roton minimum. First, note that the requirement

$$\frac{1}{2} \sum_{\alpha=1,2} \boldsymbol{\eta}_\alpha^T \hat{\mathbf{M}} \boldsymbol{\eta}_\alpha > 0 \quad (59)$$

with  $\boldsymbol{\eta}_\alpha^T = (\varepsilon_{\alpha 3}, \varepsilon_{3\alpha}, \gamma_{\alpha 3})$ , implies  $\det \hat{\mathbf{M}} > 0$ . Next, from the dispersion relation (37) it can be readily established that the roton minimum touches zero provided  $a_\alpha b_\alpha = \Delta_\alpha^2$ , where  $\alpha = \pm$ . This condition maintains

$$(A_{55} B_{44} - C_{74}^2) k^2 \mp 2(A_{55} C_{44} - A_{47} C_{74}) k + A_{44} A_{55} - A_{47}^2 = 0. \quad (60)$$

It is straightforward to show that

$$D/4 = -A_{55} \det \hat{\mathbf{M}}. \quad (61)$$

Because  $A_{55}$  must be positive, the stability condition,  $\det \hat{\mathbf{M}} > 0$ , leads to  $D < 0$ , i.e., Eq. (60) has no nontrivial solutions for  $k$ . Therefore, the roton minimum never touches zero and a "roton" instability of the crystalline order never occurs.